SHIRMS 2008 – Y. Potvin, J. Carter, A. Dyskin, R. Jeffrey (eds)

doi:10.36487/ACG_repo/808_46

Rotational Mechanism of In-Plane Shear Crack Growth in Rocks Under Compression

A.V. Dyskin *School of Civil and Resource Engineering, The University of Western Australia, Australia*

E. Pasternak *School of Mechanical Engineering, The University of Western Australia, Australia*

Abstract

In-plane growth of shear fractures in rocks in the presence of high magnitude compression routinely observed in both laboratory testing and in the field so far eludes explanation. Indeed, in-plane growth of shear crack is difficult to explain based on the Linear Elastic Fracture Mechanics. We propose here a mechanism that reconciles the observations and the theory. We assume that what presents itself as a Mode II crack is in fact a crack driven by relative rotations of grains at the crack tip. The relative rotations are created by the conventional shearing of the crack faces, which leads to a concentration of moment stresses at the crack tip. The moment stress – the bending moment per unit area created in the intergranular bonding due to the relative rotation of the grains – ruptures the bonds in front of the crack creating en-echelon formation. This affects the in-plane growth when the conventional out-of-plane growth (kinking) caused by the concentration of tensile stress is suppressed by the high ambient compression.

1 Introduction

Failure of rocks and rock masses often occurs in the form of shear fracture propagating in its own plane. Direct laboratory experiments however strongly suggest that locally the fractures are initiated only through the action of tensile stresses. In the case of an initial crack inclined to the axis of the highest compression this always results in the formation of wing cracks growing in the direction of that axis. This leaves open the question as to what the mechanism of shear failure is. In order to answer this question we invoke the following observations: (a) after the wing cracks are formed and exhaust their ability for further growth - due to either the lateral constraint or the intrinsic limitations (Dyskin et al., 1994; 2003), secondary fractures are formed and propagate in the direction of the original shear crack (Bobet, 2000); (b) under closer look these fractures appear to consist of a row of microcracks making an impression of en-echelon formation; (c) these additional fractures appear only in heterogeneous rock-like materials, never being observed in homogeneous brittle materials.

A popular perception is that the mechanism of growth of shear crack in its own plane is the formation of en-echelon structure of small tensile microcracks which collectively behave as a macroscopic shear fracture, Figure 1. The en-echelon microcracks are believed to be formed by the local tensile stresses induced by the singular shear stress, Figure 1. The role of the nucleus for these microcracks is played by the pre-existing cracks and the inter-grain boundaries.

A key point in analysing this concept is the abovementioned observation that the in-plane growth of artificial shear cracks is an attribute of heterogeneous brittle materials and never the homogeneous ones. However, the homogeneous materials only appear to be such at the scale of observation: at the microlevel they have different types of defects. If the conventional en-echelon explanation is correct and the tensile stresses induced by the shear stress singularity can produce en-echelon forming microcracks at the inter-grain boundaries then the same should happen in the so called homogeneous materials, but at the microlevel. The fact that this is not observed may only mean that the small weak planes or defects are not sufficient for the en-echelon formation. It should be further noted that the heterogeneous materials in which the in-plane shear crack growth is observed are in fact particulate materials which consist of cemented grains or particles. These particles have also an ability to rotate relative to each other and thus bend the bonds between them. Under this bending the bonds can rupture without application of external tensile stresses and thus constitute a mechanism of crack growth. (Of course, the bond rupture in bending involves local tensile stresses, but they are balanced out by local compressive stresses such that the total, macroscopic stress is zero.) Therefore,

understanding of the mechanics of local rotations and bending moments is a basis for realistic modelling of shear failure of rocks. This paper attempts to model the fracture propagation associated with local rotations.

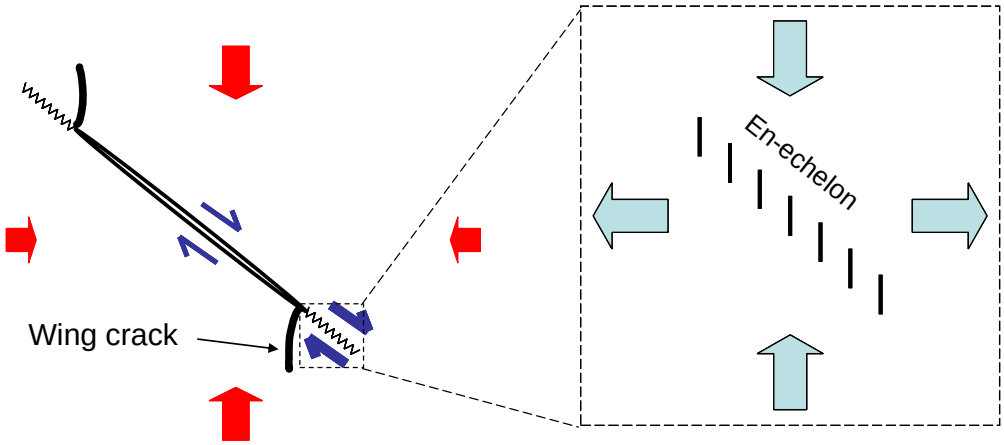

Figure 1 A conventional concept of en-echelon mechanism of in-plane growth of initial inclined crack; en-echelon is formed as a continuation of the initial crack

Capturing the field of relative rotations and the associated moment stresses is beyond the resolution of the classical continuum theories (regardless of the constitutive relationships assumed), since there exist only three translational degrees of freedom within the framework of the classical continuum. The simplest generalisation which captures the rotational degrees of freedom and the effects of relative (grain) rotations and moment stresses is provided by the Cosserat continuum. In Section 2 we briefly introduce the Cosserat continuum and infer the characteristics of the Cosserat constitutive relationship (Cosserat moduli) from the grain size and the properties and sizes of the cement bonds. We use the homogenisation by differential expansion method (Pasternak and Mühlhaus, 2005). In Section 3 we use a two-dimensional (2D) approximation and determine the characteristic lengths of the continuum. In Section 4 we proceed with the analysis of the mechanics of crack growth associated with the grain rotations. This rotational mechanism of crack growth essentially constitutes the cracks of higher modes on top of the conventional Mode I (tensile) and Modes II and III (shear) cracks (Pasternak et al., 2006a). In Section 5 we introduce the key point which enabled a breakthrough in the analysis of crack propagation in the Cosserat continuum – an intermediate asymptotics of distances smaller than the crack length but larger than the grain size. This is a crucial approximation allowing the problem of moment stress singularity to be addressed and the criterion of shear crack propagation to be formulated. Finally, in Section 6, we formulate the criterion of crack propagation and demonstrate the importance of the introduced mechanism as compared to the traditional one.

2 Cosserat continuum model of rock

The proposed approach assumes that the brittle rock is elastic. Subsequently we treat the rock as an assembly of particles connected by elastic bonds which represent the interparticle cement layers. As a further simplification, we will neglect the shape of the grains and model them by spherical particles. This is a considerable simplification as it neglects the effect of elbowing of rotating non-spherical particles. (In the first approximation this effect adds additional non-linear resistance to the relative rotations (Pasternak et al., 2006b) and can be accounted by the corresponding adjustment of the rotational stiffnesses.) Furthermore the rock will be assumed isotropic. Thus we arrive at the model, Figure 2, consisting of rigid spherical particles of the same diameter, D, each pair being connected by a set of normal, shear and rotational springs. Subsequently, each connection is represented by two sets of three mutually perpendicular springs: the conventional set of a normal and two shear (tangential) springs and the set of three rotational springs – a torsional and two bending springs. We note that the springs are characterised by the stiffnesses with the units $[k_n] = [k_s]$ = N/m for the conventional springs and $[k_{\varphi_n}] = [k_{\varphi_s}]$ = N·m for the rotational ones.

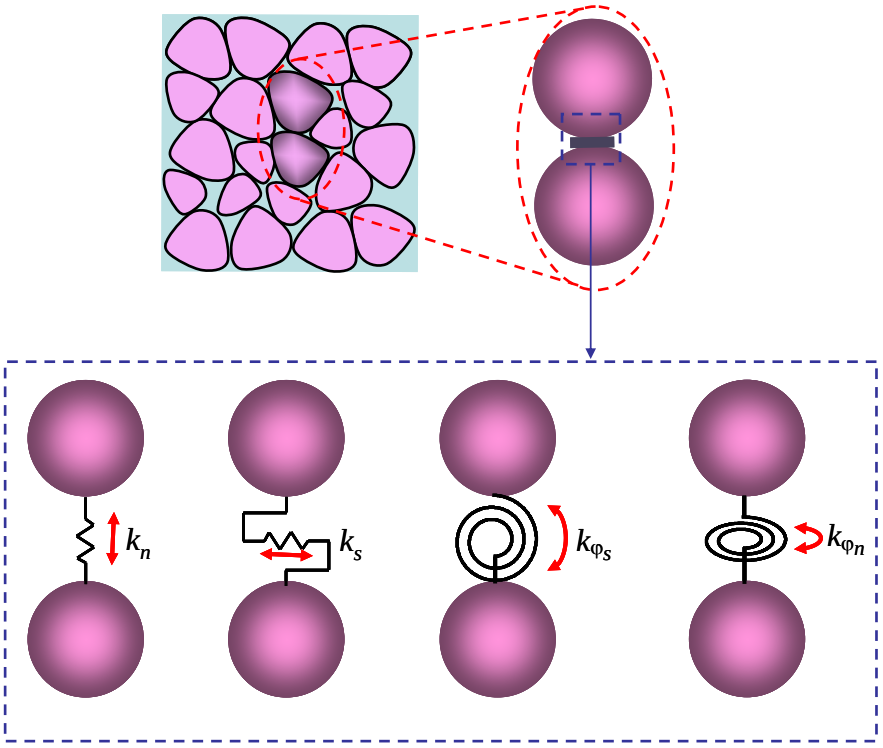

Figure 2 **Model of rock based on assembly of identical spheres connected by the normal (k_n), shear (k_s), bending (k_{φ_s}), and torsional (k_{φ_n}) springs. For each k_s and k_{φ_s} spring there is a similar spring (not shown in the picture) that provides resistance to shearing and bending in the plane normal to the plane of drawing**

Stiffnesses of the springs are estimated by visualising the (cement) bond as a cylinder of height h and radius b loaded either by uniform loads (for the normal and shear stiffnesses) or linearly distributed loads with vanishing average (for the rotational stiffnesses), Figure 3. We also assume that other normal stress components vanish: $\sigma_{11} = \sigma_{22} = 0$. Assuming the material of the bonds (cement) to be isotropic with the Young's modulus and shear modulus E_b and G_b and calculating the corresponding total force and moment for the applied stress distributions and the resulting displacement distributions we find the stiffnesses that define the force-displacement and moment-rotation responses of the bonds:

$$k_n = \frac{\pi b^2 E_b}{h}, \quad k_s = \frac{\pi b^2 G_b}{h}, \quad k_{\varphi_n} = \frac{\pi b^4 G_b}{2h}, \quad k_{\varphi_s} = \frac{\pi b^4 E_b}{4h} \tag{1}$$

Using these stiffnesses the force and moment tensors could be expressed through relative displacement $\Delta\overset{\rho}{u}$ and rotation $\Delta\overset{\rho}{\phi}$ of the ends of the bonds as follows (Pasternak et al., 2004):

$$\overset{\rho}{F} = K\Delta\overset{\rho}{u}, \ \overset{\rho}{M} = L\Delta\overset{\rho}{\phi} \tag{2}$$

where:

$$K = \left[K_{ij}\right], \ K_{ij} = \left(k_n - k_s\right)n_i n_j + k_s\delta_{ij}, \ L = \left[L_{ij}\right]$$
$$L_{ij} = \left(k_{\varphi_n} - k_{\varphi_s}\right)n_i n_j + k_{\varphi_s}\delta_{ij} \tag{3}$$

Here K and L are the matrices of the translational and rotational spring stiffnesses with components K_{ij} and L_{ij} respectively, while k_n, k_s and k_{φ_n}, k_{φ_s} can be called the normal and shear (tangential) contact stiffnesses of the translational and rotational springs. The indices i, j refer to a spatially fixed Cartesian coordinate system (x_1, x_2, x_3), Figure 3.

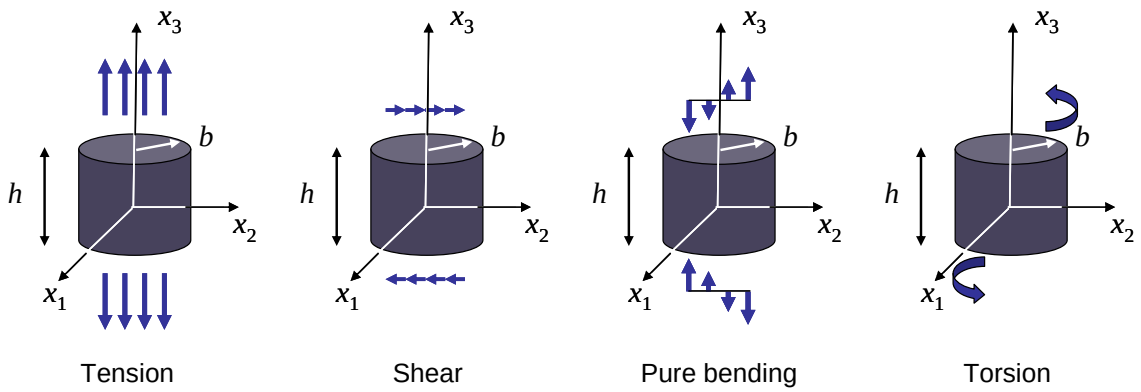

Figure 3 Schematics of estimation of the bond stiffnesses. The Cartesian coordinate frame shown is local to the bond

Assuming that the particle arrangements are statistically homogeneous and applying the method of homogenisation by differential expansions (Pasternak et al., 2004; Pasternak and Mühlhaus, 2005) one obtains the following equations of equilibrium:

$$\sigma_{ji,j} = 0\,,\ \mu_{ji,j} + \varepsilon_{ijk}\sigma_{jk} = 0_i \tag{4}$$

and constitutive equations:

$$\sigma_{ji} = C_{ijlm}\gamma_{lm} + C_{lj}\gamma_{li}\,,\ \mu_{ji} = D_{ijlm}\kappa_{lm} + D_{lj}\kappa_{li} \tag{5}$$

Here σ_{ij} and μ_{ij} are the tensors of non-symmetric stress and moment stress respectively, ε_{ijk} is the alternating matrix, γ_{ij} and κ_{ij} are the conventional Cosserat continuum deformation measures (Nowacki, 1974):

$$\gamma_{ji} = u_{i,j} - \varepsilon_{kji}\varphi_k\,,\ \kappa_{ji} = \varphi_{i,j} \tag{6}$$

where φ_i is the Cosserat rotation, γ_{ji} and κ_{ji} are the strain and curvature twist.

The parameters of the constitutive relationships Equation (5), which can be referred to as the non-standard elastic moduli C_{ijlm}, C_{lj}, D_{ijlm}, D_{lj} have the form:

$$C_{ijlm} = \frac{6\nu_s}{\pi D}(k_n - k_s)A_{ijlm}\,,\ C_{lj} = \frac{6\nu_s}{\pi D}k_s A_{lj}\,,\ D_{ijlm} = \frac{6\nu_s}{\pi D}\left(k_{\varphi_n} - k_{\varphi_s}\right)A_{ijlm}\,,\ D_{lj} = \frac{6\nu_s}{\pi D}k_{\varphi_s}A_{lj} \tag{7}$$

where ν_s is the volumetric fraction of grains, D is the grain diameter, and k is the coordination number (the average number of contacts). Tensors A_{lj} and A_{ijlm} depend upon the distribution of contacts. For isotropic rock the model is characterised by isotropic distribution of particle contacts, $A(\vec{r},\vec{n}) = k/4\pi$, hence:

$$A_{lj} = \int_{\alpha/2} A n_l n_j dn = \frac{k}{6}\delta_{lj}\,,\ A_{ijlm} = \int_{\alpha/2} A n_i n_j n_l n_m dn = \frac{k}{30}\{\delta_{ij}\delta_{lm} + \delta_{il}\delta_{jm} + \delta_{im}\delta_{jl}\} \tag{8}$$

Here δ_{ij} is the Kronecker delta.

The Lamé equations can be obtained in the usual way by substituting Equation (6) into Equation (5) and then the result into Equation (4). In the following section we concentrate on a 2D approximation of this theory which will be necessary for the crack analysis.

3 2D approximation

Now we consider a two dimensional Cosserat continuum in plane (x_1, x_2). The expression of the constitutive law for isotropic 2D Cosserat continuum reads (Nowacki, 1974):

$$\begin{aligned}
&\sigma_{11} = (2\mu + \lambda)\gamma_{11} + \lambda\gamma_{22}, \quad \sigma_{12} = (\mu + \alpha)\gamma_{12} + (\mu - \alpha)\gamma_{21} \\
&\sigma_{21} = (\mu + \alpha)\gamma_{21} + (\mu - \alpha)\gamma_{12}, \quad \sigma_{22} = \lambda\gamma_{11} + (2\mu + \lambda)\gamma_{22} \\
&\mu_{13} = B\kappa_{13}, \quad \mu_{23} = B\kappa_{23}
\end{aligned} \tag{9}$$

where the Cosserat deformation measures – strains γ_{ji} and curvatures κ_{ji} – are given by Equation (6).

By rewriting Equation (5) for 2D approximation and comparing it with Equation (9), the Cosserat elastic moduli can be expressed through stiffnesses, Equation (1), grain diameter and volumetric fraction:

$$\lambda = \frac{\nu_s k(k_n - k_s)}{5\pi D}, \quad \mu = \frac{\nu_s k(2k_n + 3k_s)}{10\pi D}, \quad \alpha = \frac{\nu_s k k_s}{2\pi D}, \quad B = \frac{\nu_s k(k_{\varphi_n} - k_{\varphi_s})}{5\pi D} \tag{10}$$

The Lamé constants λ and μ, as well as the Cosserat modulus α have units of stress, while the bending stiffness B has units of stress times length squared. Therefore parameters of unit of length can be constructed from the moduli playing the role of internal characteristic lengths. In the isotropic case there are two independent parameters:

$$l_1 = \sqrt{\frac{B}{4\mu}}; \quad l_2 = \sqrt{\frac{B}{4\alpha}}; \quad l = \sqrt{l_1^{\,2} + l_2^{\,2}} \tag{11}$$

We express them through the bond stiffnesses and the bond parameters (moduli and diameter) as follows:

$$l_1 = \sqrt{\frac{B}{4\mu}} = \sqrt{\frac{k_{\varphi_n} + 4k_{\varphi_s}}{2(2k_n + 3k_s)}} = \frac{1}{2} b \sqrt{\frac{2E_b + G_b}{2E_b + 3G_b}}; \quad l_2 = \sqrt{\frac{B}{4\alpha}} = \sqrt{\frac{k_{\varphi_n} + 4k_{\varphi_s}}{10k_s}} = b\sqrt{\frac{2E_b + G_b}{20G_b}} \tag{12}$$

We use these characteristic lengths in the following analysis.

4 Shear crack in 2D Cosserat continuum — the structure of stress concentrations

In order to decipher a possible mechanism of crack growth one needs to identify the non-zero components of stress and moment stress acting at the crack tip. This can be done for a general case invoking the symmetry considerations as follows. Consider a crack shown in Figure 4 and note that the crack's geometry is symmetrical with respect to the coordinate transformation $x_2 \rightarrow -x_2$. Under this transformation all tensorial quantities which contain index 2 even number of times (or do not contain at all), such as normal stresses, do not change the sign, while the tensorial quantities which contain index 2 odd number of times (like shear stress) change the sign. On top of that, under this transformation the coordinate frame changes the orientation from the right-handed to the left-handed. This results in the pseudo-tensorial quantities (moment stress) changing the sign once more. Therefore the coordinate transformation leads to:

$$\sigma_{11} \rightarrow \sigma_{11}, \quad \sigma_{22} \rightarrow \sigma_{22}, \quad \sigma_{12} \rightarrow -\sigma_{12}, \quad \mu_{13} \rightarrow -\mu_{13}, \quad \mu_{23} \rightarrow \mu_{23} \tag{13}$$

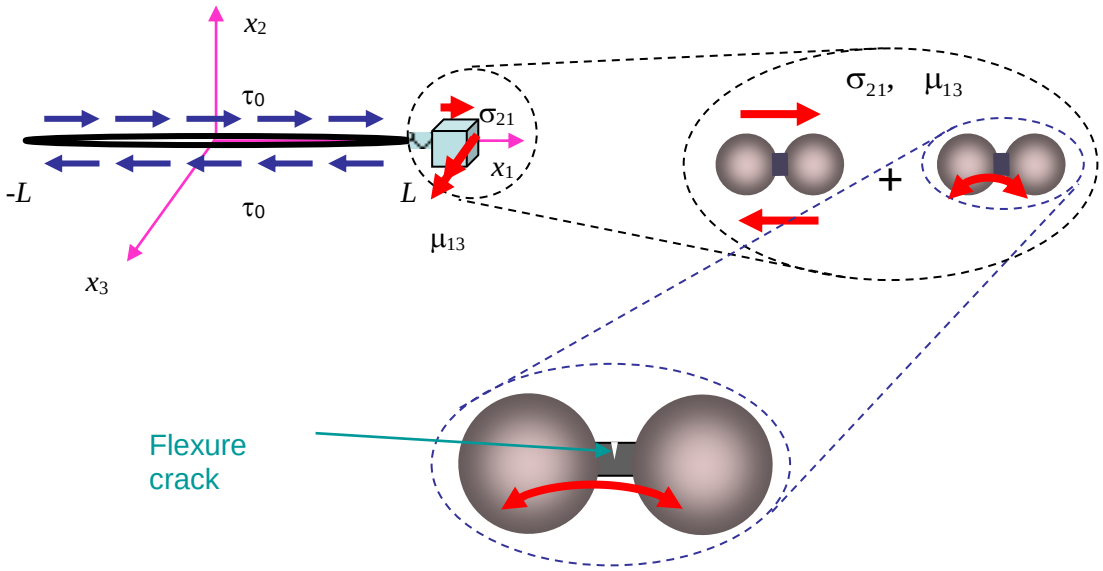

Figure 4 2D crack under shear load and the stress components at the point of crack continuation; moment stresses inducing flexure cracks

We consider these stress components at the points of the x_1-axis; these points are invariant under the above transformation. We note that since under this transformation the loading parameter changes sign $\tau_0 \to -\tau_0$ all stress and moment stress must change the sign too. Therefore, all stress and moment stress components which do not change the sign under the transformation must vanish:

$$\sigma_{11} = \sigma_{22} = 0, \quad \mu_{23} = 0 \text{ along } x_1 \tag{14}$$

It follows from here that only two stress components act at the points of the crack continuation, Figure 4: the conventional shear stress σ_{21} and the moment stress μ_{13}. The latter is capable of inducing bending in the inter-grain bond and creating vertical cracks (Figure 4) that form en-echelon observed by Bobet (2000). In order to understand the distribution of the moment stress and the order of singularity we have to consider the 2D problem of shear crack in Cosserat continuum. As such a problem has no closed form solution we consider an asymptotic solution referring to small Cosserat length scale.

5 Asymptotics of small Cosserat lengths

A distinctive advantage of the (elastic) Cosserat continuum description over the classical elastic one is the presence of internal lengths which provide the first approximation account for the material microstructure. As seen from Section 2 the characteristic length, l, is of the order of the bond radius b, which in its turn is of the order of the grain size. This provides the key point to our model: because the Cosserat (or any other) continuum is an approximation to the real material based on the introduction of the representative volume element, the latter is necessarily much larger than the microstructure (in this case the grain) size. The volume element size defines the resolution of the continuum model which is coarser than the grain size. Subsequently, the distances smaller than the grain size or for that matter smaller than the Cosserat characteristic length is beyond the resolution of the continuum model. The simple consequence of this consideration is: while the Cosserat continuum formally allows addressing any distances (it is a continuum after all), lengths smaller than the characteristic length cannot be made relevant to the original material. Therefore, when the stress concentration at the crack tip is considered, only the distances larger than the characteristic length can be considered.

This leads to the following intermediate asymptotics:

$$l << r << L \tag{15}$$

where, r is the distance from the crack tip, L is the crack size, Figure 5. This intermediate asymptotics should be used instead of the traditional one ($r << l$) which is commonly used in the literature (Sternberg and Muki, 1967; Atkinson and Leppington, 1977; Morozov, 1984; Nakamura and Lakes, 1988; Garajeu and Soós, 2003; Kobelev, 2006; Gourgiotis and Georgiadis, 2007; Shmoylova et al., 2007). This intermediate asymptotics is obtained in the limiting transition $r/l \to \infty$ and then formally used all the way through to $r \to 0$.

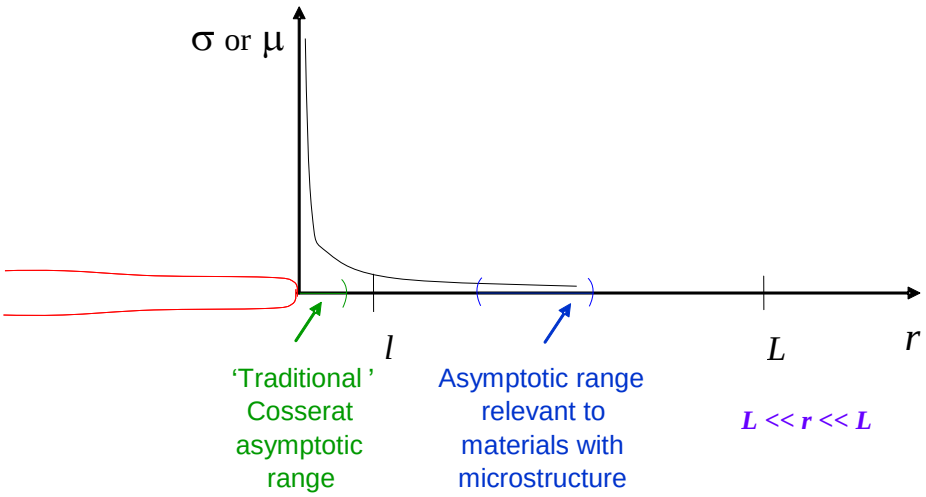

Figure 5 Area in front of the crack tip. The Cosserat characteristic length separates two asymptotic ranges: the traditional one, $r << l$ and the realistic one given by Equation (15)

By substituting the constitutive Equation (9) and expressions of deformation measures Equation (6) into the 2D equivalent of equations of equilibrium Equation (4) one obtains the Lamé equations in the form:

$$\begin{cases} (\lambda+2\mu)\left(\dfrac{\partial^2 u_1}{\partial x_1{}^2}+\dfrac{\partial^2 u_2}{\partial x_1 \partial x_2}\right)+(\mu+\alpha)\left(\dfrac{\partial^2 u_1}{\partial x_2{}^2}-\dfrac{\partial^2 u_2}{\partial x_1 \partial x_2}\right)+2\alpha\dfrac{\partial \varphi_3}{\partial x_2}=0 \\ (\lambda+2\mu)\left(\dfrac{\partial^2 u_1}{\partial x_1 \partial x_2}+\dfrac{\partial^2 u_2}{\partial x_2{}^2}\right)+(\mu+\alpha)\left(\dfrac{\partial^2 u_2}{\partial x_1{}^2}-\dfrac{\partial^2 u_1}{\partial x_1 \partial x_2}\right)-2\alpha\dfrac{\partial \varphi_3}{\partial x_1}=0 \\ l_2{}^2\left(\dfrac{\partial^2 \varphi_3}{\partial x_1{}^2}+\dfrac{\partial^2 \varphi_3}{\partial x_2{}^2}\right)-\varphi_3+\dfrac{1}{2}\left(\dfrac{\partial u_2}{\partial x_1}-\dfrac{\partial u_1}{\partial x_2}\right)=0 \end{cases} \tag{16}$$

where λ and μ are the Lamé constants (μ is the shear modulus) of the rock, α is the Cosserat shear modulus and the use of a length parameter l_2 as defined in Equation (11) was made.

Asymptotics Equation (15) implies that l_2 must be small as compared to other distances. A first approximation can be obtained through the limiting transition:

$$l_2 \to 0. \tag{17}$$

This immediately reduces the third equation from Equation (16) to:

$$\varphi_3 = \frac{1}{2}\left(\frac{\partial u_2}{\partial x_1}-\frac{\partial u_1}{\partial x_2}\right) \tag{18}$$

implying that the rotation is no longer independent of the displacement. Therefore the asymptotics of small characteristic size formally leads to the Cosserat continuum with constrained rotations. We can now capitalise on the solutions developed for this simpler model and obtain the necessary asymptotic solutions for the full Cosserat continuum.

6 Shear and moment stress concentration at the crack tip

Consider a shear crack of length $2L$ under uniform loading, Figure 4. The boundary conditions for this problem are:

$$\sigma_{21} = \tau_0, \quad \sigma_{22} = 0, \quad \mu_{23} = 0 \quad \text{for} \quad -L \le x_1 \le L, \quad x_2 = 0 \tag{19}$$

and stresses and displacements are continuous outside the segment [-*L*, *L*].

A standard method of addressing a crack problem consists of representing the crack as a continuous distribution of dislocations (displacement discontinuities) and disclinations (rotation discontinuities in the case of Cosserat continuum) of unknown density in the otherwise continuous material and then equating the stress produced by all dislocations at the points of the crack contour to the boundary conditions. For the boundary conditions Equation (19) this leads to the following system of (singular) integral equations for unknown dislocation $\rho_1(x)$ and disclination $\rho_3(x)$ densities:

$$\begin{aligned} &\int_{-L}^{L}\left[K_{21}(x-\xi)\rho_1(\xi)+K_{23}(x-\xi)\rho_3(\xi)\right]d\xi = \tau_0 \\ &\int_{-L}^{L}\left[M_{21}(x-\xi)\rho_1(\xi)+M_{23}(x-\xi)\rho_3(\xi)\right]d\xi = 0 \end{aligned} \tag{20}$$

Here $K_{21}(x)$ and $M_{21}(x)$ are the shear stress σ_{21} and moment stress μ_{23} created at point x (on x_1-axis) by a dislocation of unit Burgers vector b={1,0,0} situated at the origin; $K_{23}(x)$ and $M_{23}(x)$ have similar meaning for disclinations (Burgers vector b={0,0,1}). (We note that the units of Burgers vectors are meters for dislocations and radians for disclinations.) Equation (20) is complemented by the conditions of single-valuedness of displacements and rotations.

From solution of Equation (20) the stress field around the crack can be computed by summing up the stresses produced by individual dislocations and disclinations. Thus the key point here is the expression for stresses generated by a dislocation and disclination with a given Burgers vector b required to determine the kernes in Equation (20).

We start with the dislocation. Asymptotics Equation (15) formally reduced the Cosserat continuum to the Cosserat continuum with constrained rotations. A solution for the x_1-dislocation (b={1,0,0}) in this continuum was obtained by Gourgiotis and Georgiadis (2007):

$$\sigma_{11} = -\frac{\mu b\left(3\sin\theta+\sin 3\theta\right)}{4\pi(1-\nu)r} + \frac{2\mu b}{\pi r}\left[\frac{2l^2}{r^2} - K_2\left(\frac{r}{l}\right)\right]\sin 3\theta - \frac{\mu b r}{\pi l^2}\left[K_2\left(\frac{r}{l}\right) - K_0\left(\frac{r}{l}\right)\right]\left(\sin\theta+\sin 3\theta\right)$$

$$\sigma_{22} = \frac{\mu b\left(\sin 3\theta-\sin\theta\right)}{4\pi(1-\nu)r} - \frac{2\mu b}{\pi r}\left[\frac{2l^2}{r^2} - K_2\left(\frac{r}{l}\right)\right]\sin 3\theta + \frac{\mu b r}{\pi l^2}\left[K_2\left(\frac{r}{l}\right) - K_0\left(\frac{r}{l}\right)\right]\left(\sin\theta+\sin 3\theta\right)$$

$$\sigma_{12} = \frac{\mu b\left(\cos\theta+\cos 3\theta\right)}{4\pi(1-\nu)r} - \frac{2\mu b}{\pi r}\left[\frac{2l^2}{r^2} - K_2\left(\frac{r}{l}\right)\right]\cos 3\theta - \frac{\mu b r}{\pi l^2}\left[K_2\left(\frac{r}{l}\right) - K_0\left(\frac{r}{l}\right)\right]\left(\cos\theta-\cos 3\theta\right)$$

$$\sigma_{21} = \frac{\mu b\left(\cos\theta+\cos 3\theta\right)}{4\pi(1-\nu)r} - \frac{2\mu b}{\pi r}\left[\frac{2l^2}{r^2} - K_2\left(\frac{r}{l}\right)\right]\cos 3\theta + \frac{\mu b r}{\pi l^2}\left[K_2\left(\frac{r}{l}\right) - K_0\left(\frac{r}{l}\right)\right]\left(\cos\theta+\cos 3\theta\right)$$

$$\mu_{13} = \frac{\mu b}{\pi}\left[\frac{2l^2}{r^2} - K_2\left(\frac{r}{l}\right)\right]\cos 2\theta - \frac{\mu b}{\pi}K_0\left(\frac{r}{l}\right), \quad \mu_{23} = \frac{\mu b}{\pi}\left[\frac{2l^2}{r^2} - K_2\left(\frac{r}{l}\right)\right]\sin 2\theta$$

Here b is the respective non-zero component of the Burgers vector, $r^2 = x_1^2 + x_2^2$, θ is the polar angle; $K_m(r)$ is the m-th modified Bessel function of the second kind.

As discussed above, we are interested in the asymptotics $r >> l$. For large r the modified Bessel functions vanish exponentially, so as $r/l \to \infty$ the main asymptotic terms are proportional to r^{-1}. Neglecting the higher order terms we obtain the corresponding asymptotic expressions. (In the language of the method of matching

asymptotics they represent the outer asymptotics. We then use the inner asymptotics, $r \to 0$ to obtain the kernes in Equation (20), in the spirit of Pasternak et al. (2006c).) Thus we have the following asymptotics:

$$\sigma_{11} = -\frac{\mu b(3\sin\theta + \sin 3\theta)}{4\pi(1-\nu)r},\ \sigma_{22} = \frac{\mu b(\sin 3\theta - \sin\theta)}{4\pi(1-\nu)r},\ \sigma_{12} = \sigma_{21} = \frac{\mu b(\cos\theta + \cos 3\theta)}{4\pi(1-\nu)r} \tag{21}$$

$$\mu_{13} = \frac{\mu b}{\pi}\frac{2l^2}{r^2}\cos 2\theta, \quad \mu_{23} = \frac{\mu b}{\pi}\frac{2l^2}{r^2}\sin 2\theta \tag{22}$$

Equation (21) coincides with the solution for a conventional x_1-dislocation in the classical isotropic elastic continuum (Landau and Lifshitz, 1959). It follows from Equation (22) that the moment stress μ_{23} created by the dislocation on the crack line ($\theta = 0, \pm\pi$) is equal to zero. This means that the x_1-dislocation does not contribute to the moment stress on the crack line. Therefore the boundary conditions Equation (19) can be satisfied by the appropriate distribution of the x_1-dislocations without the need to add disclinations. (There is no coupling between the dislocations and disclination for the shear crack.) Subsequently, Equation (20) reduces to only one equation which is a conventional equation for a shear crack whose solution for a uniform load is known. Furthermore, since we are only interested in the stress concentration at the crack tip, we can obtain a general result using the expression for the displacement discontinuity at the crack tip. We use the expression for the distribution of the relevant displacement component in a vicinity of a Mode II crack tip (Tada et al., 1985).

$$u_1 = \frac{K_{II}}{\mu}\sqrt{\frac{r}{2\pi}}\sin\frac{\theta}{2}\left[2(1-\nu) + \cos^2\frac{\theta}{2}\right] \tag{23}$$

Here (r, θ) is the polar coordinate frame with the origin placed at the crack tip, Figure 6; K_{II} is the mode II stress intensity factor; ν is the Poisson's ratio of the rock. The displacement discontinuity is the difference between displacements for $\theta = \pi$ and $\theta = -\pi$; the dislocation density is the derivative (over x_1, Figure 6) thereof. The latter reads:

$$\rho_1(r) = \frac{2K_{II}(1-\nu)}{\mu\sqrt{2\pi r}} \tag{24}$$

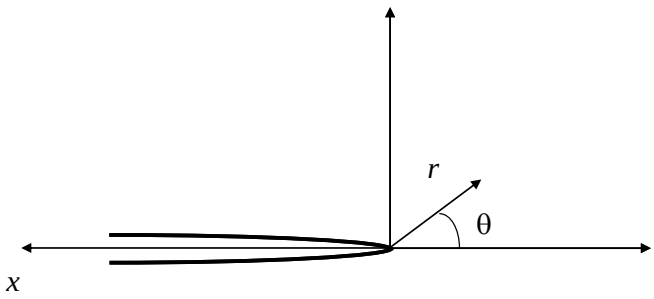

Figure 6 The coordinate systems for calculating the moment stress concentration at the crack tip

Using the expression for the dislocation-generated moment stresses Equation (22) one obtains the moment stress at the crack tip on the line of crack continuation (θ=0) whose leading asymptotic term (as $r \to 0$) reads:

$$\mu_{13} = \frac{\mu}{\pi}2l^2\int_0^{2L}\frac{\rho_1(\xi)d\xi}{(x-\xi)^2} \sim \frac{K_{II}(1-\nu)}{\sqrt{2\pi}r^{3/2}}l^2, \quad \mu_{23} = 0, \quad x = -r \tag{25}$$

We emphasise that $\mu_{23} = 0$, as derived in Section 4, but $\mu_{13} \neq 0$ and can produce en-echelon cracks.

The moment stress has a singularity of a degree higher than the conventional stress components. One should recall, however, that in this model the distances smaller than l have no physical meaning. At most one can compare the stresses at distance l from the crack tip. Subsequently, the moment stress at the crack tip can be estimated at this distance:

$$\mu_{13} \sim \frac{K_{II}(1-\nu)}{\sqrt{2\pi}}\sqrt{l} \tag{26}$$

This moment stress creates bending moment in the inter grain bonds (Figure 4). The associated maximum tensile stress can be obtained assuming the linear distribution of stress across the bond (the same way as when the bending stiffness was calculated, Figure 3). Referring the bending moment to the area of l^2 such that the bending moment $M \sim \mu_{13} l^2$ and then taking the maximum microscopic tensile stress caused by bending as $12M/l^2$ and assuming $1-\nu \sim 1$ one obtains the following estimate:

$$\sigma_{moment} \sim \frac{12K_{II}}{\sqrt{2\pi l}} \tag{27}$$

If we apply the same logic to the microscopic tensile stress caused by the conventional shear stress concentration (in the principal directions) one obtains:

$$\sigma_{conventional} \sim \frac{K_{II}}{\sqrt{2\pi l}} \tag{28}$$

Thus the stress associated with the effect of grain rotation can considerably exceed the conventional stress concentration. This is mainly due to the additional concentration of the bending stress in the bond (factor 12 in Equation (27)). Subsequently the local bond breakage by rotational mechanism (production of flexure cracks) can come well before the initiation of crack growth by conventional mechanisms. It is of course an entirely different question as to whether the local bond breakage is sufficient to initiate the crack propagation. Nevertheless, if the conventional crack growth is suppressed as often happens with crack growth in compression, the local bond breakage can take over as a mechanism of crack propagation. This situation is illustrated in Figure 7.

7 Conclusions

Heterogeneous materials with granular (particulate) microstructure, like rocks, permit relative rotations of the grains independent of their displacements. The relative rotations are induced by shear and moment stresses, the latter being the bending moments per unit area. The resistance to the rotations is controlled by the bending stiffness of the inter-grain bonds. If the bending is high enough the bonds can break causing local microcracking. Under compression, when further crack growth of an initial shear crack through tensile branching is suppressed, these bending-induced microcracks can take the lead forming en-echelon formation and thus effecting the in-plane shear crack propagation.

Modelling of this mechanism calls for the use of the Cosserat continuum to incorporate the rotational degrees of freedom and the length parameters representing the characteristic sizes of the rock microstructure. The introduction of the Cosserat continuum however implicitly involves a homogenisation procedure which introduces a representative volume element whose size must exceed the characteristic sizes of microstructure (the grain size in our case). An often overlooked implication of this is the limiting resolution of the continuum which does not recognise distances smaller than the volume element size, and therefore such distances, while formally admissible in the continuum, cannot be interpreted in terms of the original material. This has a particular importance for the stress distribution at the crack tip controlling the conditions of crack growth; the stress distribution relevant to the rock is an intermediate asymptotics which refers to the distances from the crack tip much smaller than the crack length (a usual requirement), but much larger than the grain size (or the Cosserat characteristic lengths). Thus instead of the popular crack tip singularity corresponding to the asymptotic of distances smaller than the minimum the Cosserat characteristic length, one needs to use the singularity which is a continuation of the intermediate asymptotics. Surprisingly, deriving such a singular stress field turns out to be technically much simpler than the traditional one, as the problem is formally reduced to the equations of the Cosserat continuum with constrained rotations for which

only far-field asymptotics has to be obtained. In the particular case of shear crack the stresses are the same as for the crack in a classical continuum, while the moment stress distribution is easily derived from the conventional displacement distribution obtained in the classical (and already solved) crack problem.

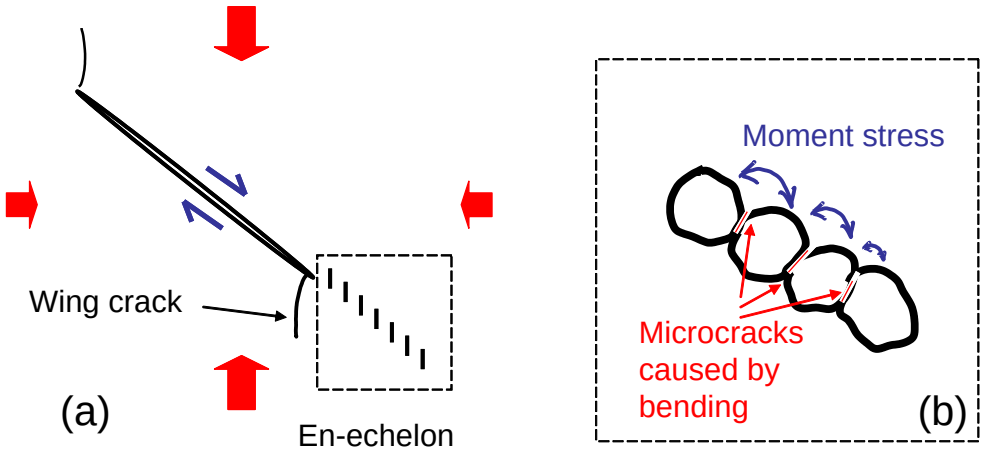

Figure 7 En-echelon mechanism of in-plane growth of initial inclined crack: (a) en-echelon formed as a continuation of the initial crack; (b) the proposed mechanism of en-echelon formation from microcracks initiated by bending of the bond layers between the grains by the concentration of moment stress at the tip of the initial crack

Direct estimates show that the local tensile stresses caused by bending related to the action of moment stresses are actually higher than the ones produced by a classical crack. This suggests that the moment stress mechanism of shear crack growth in compression can actually supersede the traditionally perceived mechanism based on the tensile stress concentration produced out of plane by shear crack and it can produce the experimentally observed in-plane growth of shear cracks.

Acknowledgements

We acknowledge the financial support from the Australian Computational Earth Systems Simulator (ACcESS), a major national research facility. The authors acknowledge the financial support from the Australian Research Council through the Discovery Grants DP0559737 and DP0773839.

References

Atkinson, C. and Leppington, F.F. (1977) The effect of couple stresses on the tip of a crack, International Journal of Solids Structures, Vol. 13, pp. 1103–1122.

Bobet, A. (2000) The initiation of secondary cracks in compression. Engineering Fracture Mechanics, 66, pp. 187–219.

Dyskin, A.V., Jewell, R.J., Joer, H., Sahouryeh, E. and Ustinov, K.B. (1994) Experiments on 3-d crack growth in uniaxial compression. International Journal of Fracture, 65 (4), pp. R77–R83.

Dyskin, A.V., Jewell, R.J., Joer, H., Sahouryeh, E. and Ustinov, K.B. (2003) Influence of shape and locations of initial 3-D cracks on their growth in uniaxial compression. Engineering Fracture Mechanics, 70(15), pp. 2115–2136.

Garajeu, M. and Soós, E. (2003) Cosserat models versus crack propagation. Mathematics and Mechanics of Solids, pp. 189–218.

Gourgiotis, P.A. and Georgiadis, H.G. (2007) Distributed dislocation approach for cracks in couple-stress elasticity: shear modes. International Journal of Fracture, 147, pp. 83–102.

Kobelev, V. (2006) Mircopolar model of fracture for composite material. Meccanica, 41, pp. 653–660.

Landau, L.D. and Lifshitz, E.M. (1959) Theory of Elasticity, Oxford. London. Edinburgh. New York. Toronto. Sydney. Paris. Braunschweig, 165 p.

Morozov, N.F. (1984) Mathematical Issues of the Crack Theory, Nauka, Moscow (in Russian), 255 p.

Nakamura, S. and Lakes, R.S. (1988) Finite element analysis of stress concentration around a blunt crack in a Cosserat elastic solid. Computer Methods in Applied Mechanics and Engineering, 66, pp. 257–266.

Nowacki, W. (1974) The linear theory of micropolar elasticity. Micropolar Elasticity, W. Nowacki and W. Olszak (editors), Wien, New York: Springer Verlag, pp.1–43.

Pasternak, E., Mühlhaus, H.-B. and Dyskin, A.V. (2004) On the possibility of elastic strain localisation in a fault. Pure and Applied Geophysics, 161, pp. 2309–2326.

Pasternak, E. and Mühlhaus, H.-B. (2005) Generalised homogenisation procedures for granular materials, Engineering Mathematics, 52(1), pp. 199–229.

Pasternak, E., Dyskin, A.V. and Mühlhaus, H.-B. (2006a) Cracks of higher modes in Cosserat continua. International Journal of Fracture, 140, pp. 189–199.

Pasternak, E., Dyskin, A.V. and Estrin, Y. (2006b) Deformations in transform faults with rotating crustal blocks. Pure and Applied Geophysics, 163, pp. 2011–2030.

Pasternak, E., Dyskin, A.V. and Mühlhaus, H.-B. (2006c) Cracks of higher modes in Cosserat continua. International Journal of Fracture, 140, pp. 189–199.

Shmoylova, E., Potapenko, S. and Rothenburg, L. (2007) Boundary element analysis of stress distribution around a crack in plane micropolar elasticity. International Journal of Engineering Science, 45, pp. 199–209.

Sternberg, E. and Muki, R. (1967) The effect of couple stress on the stress concentration of a crack. International Journal of Solids Structures, 3, pp. 69–95.

Tada, H., Paris, P.C. and Irwin, G.R. (1985) The stress analysis of cracks. Handbook. Third edition. New York: ASME Press, 512 p.